Chemical Science

EDGE ARTICLE

View Article Online
View Journal | View Issue



Cite this: *Chem. Sci.*, 2015, **6**, 4519

# Direct interfacial $Y_{731}$ oxidation in $\alpha_2$ by a photo$\beta_2$ subunit of *E. coli* class Ia ribonucleotide reductase†

David Y. Song,[a] Arturo A. Pizano,[a] Patrick G. Holder,[a] JoAnne Stubbe*[b] and Daniel G. Nocera*[a]

Received 28th March 2015
Accepted 6th June 2015

DOI: 10.1039/c5sc01125f

www.rsc.org/chemicalscience

Proton-coupled electron transfer (PCET) is a fundamental mechanism important in a wide range of biological processes including the universal reaction catalysed by ribonucleotide reductases (RNRs) in making *de novo*, the building blocks required for DNA replication and repair. These enzymes catalyse the conversion of nucleoside diphosphates (NDPs) to deoxynucleoside diphosphates (dNDPs). In the class Ia RNRs, NDP reduction involves a tyrosyl radical mediated oxidation occurring over 35 Å across the interface of the two required subunits ($\beta_2$ and $\alpha_2$) involving multiple PCET steps and the conserved tyrosine triad [$Y_{356}(\beta_2)$–$Y_{731}(\alpha_2)$–$Y_{730}(\alpha_2)$]. We report the synthesis of an active photochemical RNR (photoRNR) complex in which a Re(I)-tricarbonyl phenanthroline ([Re]) photooxidant is attached site-specifically to the Cys in the $Y_{356}$C-($\beta_2$) subunit and an ionizable, 2,3,5-trifluorotyrosine (2,3,5-$F_3$Y) is incorporated in place of $Y_{731}$ in $\alpha_2$. This intersubunit PCET pathway is investigated by ns laser spectroscopy on [$Re_{356}$]-$\beta_2$:2,3,5-$F_3Y_{731}$-$\alpha_2$ in the presence of substrate, CDP, and effector, ATP. This experiment has allowed analysis of the photoinjection of a radical into $\alpha_2$ from $\beta_2$ in the absence of the interfacial $Y_{356}$ residue. The system is competent for light-dependent substrate turnover. Time-resolved emission experiments reveal an intimate dependence of the rate of radical injection on the protonation state at position $Y_{731}(\alpha_2)$, which in turn highlights the importance of a well-coordinated proton exit channel involving the key residues, $Y_{356}$ and $Y_{731}$, at the subunit interface.



## Introduction

Enzymatic control of coupled proton and electron transfer[1–4] is critical in managing biological processes ranging from energy storage (photosystem II)[5–9] and conversion (cytochrome c oxidase)[10] to the synthesis of DNA precursors (ribonucleotide reductase).[11–14] To better understand biological PCET, we have undertaken studies of this process in class Ia RNRs, which catalyse the conversion of nucleoside diphosphates (NDPs) to deoxynucleoside diphosphates (dNDPs)—a process required for synthesis and repair of DNA in all organisms.[15,16] Catalysis by the class I RNRs proceeds by a radical mechanism requiring coupling of radical transport over 35 Å involving PCET across the two subunits to substrate turnover. The long distance, reversibility, and rate-limiting conformational gating of radical transport have made study of this process challenging. To overcome this challenge, we have developed two methodologies: photoRNRs[17–21] and site-specific incorporation of unnatural amino acids in place of pathway residues.[22–24]

*E. coli* class Ia RNR has served as the paradigm for this long distance radical transport. It is composed of two homodimeric subunits: $\alpha_2$ and $\beta_2$. A docking model for this complex,[25] substantiated by recent biochemical and biophysical studies,[26,27] has provided the working model for the radical transport pathway shown in Fig. 1. The active site for NDP reduction resides in $\alpha_2$, where the cysteine radical ($C_{439}^{\bullet}$) must be transiently generated during each turnover by the essential diferric-tyrosyl radical ($Y_{122}^{\bullet}$) cofactor in $\beta_2$. This long range oxidation requires a multi-step radical hopping mechanism that involves a specific pathway including four tyrosines ($Y_{122}$ and $Y_{356}$ in $\beta_2$; $Y_{731}$ and $Y_{730}$ in $\alpha_2$)[11,28] and potentially $W_{48}$ in $\beta_2$.[11]

Recent attention has focused on the detection of the proposed transient radical intermediates and identification of the operative PCET mechanism at each site. Mössbauer studies have established that $Y_{122}^{\bullet}$ reduction in $\beta_2$ is triggered by binding of substrate and effector to $\alpha_2$ [29] and involves proton donation from the water at $Fe_1$ (Fig. 1). This process involves orthogonal PCET wherein the proton and electron come from different residues. High-field electron paramagnetic resonance (Hf EPR) and deuterium electron nuclear double resonance (ENDOR) have provided atomic level resolution of local hydrogen bond interactions, specifically the co-linearity of the

[a]*Department of Chemistry and Chemical Biology, 12 Oxford Street, Cambridge, MA 02138-2902, USA. E-mail: dnocera@fas.harvard.edu*

[b]*Department of Chemistry, Massachusetts Institute of Technology, 77 Massachusetts Avenue, Cambridge, MA 02139-4307, USA. E-mail: stubbe@mit.edu*

† Electronic supplementary information (ESI) available: Experimental procedures, calculation of uncertainty in data analysis, purity gels, determination of $K_D$, spectroscopic characterization, time-resolved emission decay traces, and table from reference S8 are provided. See DOI: 10.1039/c5sc01125f

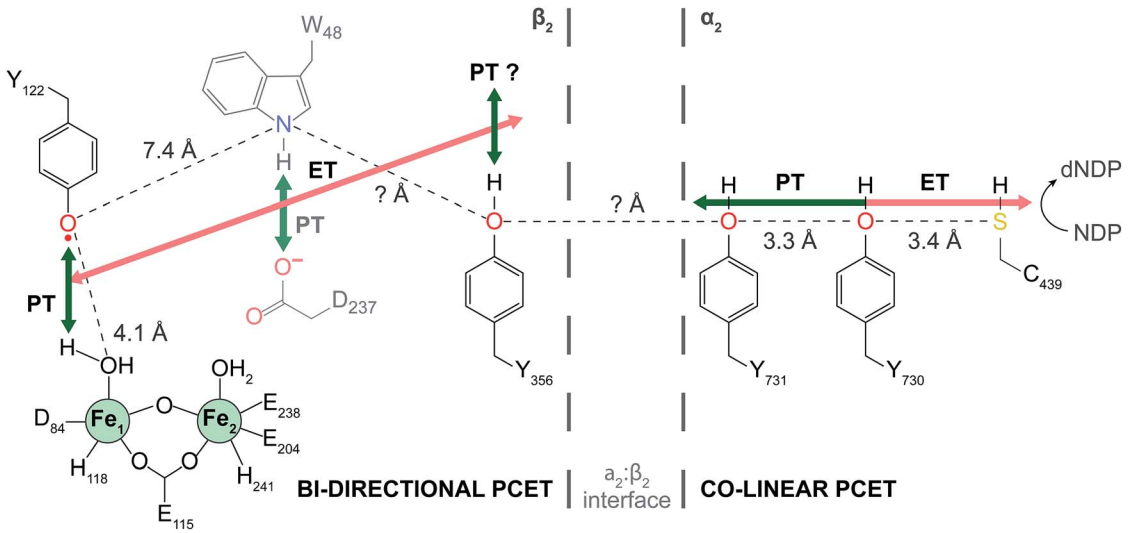


Fig. 1 Current model of radical transport pathway in class Ia RNR leading to nucleotide reduction as determined by the docking model[16] and diagonal distance measurements acquired by PELDOR spectroscopy.[34] Key redox active amino acids and known distance measurements involved in PCET pathway are shown. Residue $W_{48}$ is grayed indicating the absence of experimental evidence supporting its participation in the PCET radical mechanism. Residue $Y_{356}$ is shown at the interface for illustrative purposes. Salmon arrows indicate electron transfer (ET) and green arrows represent proton transfer (PT). In $\alpha_2$, co-linear PCET is denoted by the dual-colored arrow, and the proposed bi-directional PCET in $\beta_2$ is indicated by the orthogonality of the ET and PT pathways.

PCET within $\alpha_2$. Additionally, significant shifts in $g_x$ values together with the assignment of hyperfine coupling features from the ENDOR spectra of various amino-substituted RNR mutants propose an important role for electrostatics at the $\alpha_2$:$\beta_2$ interface.[30] However, the disordered C-terminal tail of $\beta_2$ where $Y_{356}$ resides has made interrogation of the chemistry at the subunit interface challenging (Fig. 1).

Rate limiting conformational gating in RNR obscures radical transport across the subunit interface, prompting us to develop photoRNRs to trigger radical initiation with light to avoid this gating and to potentially enable the observation of Y˙ at the interface. Radical injection kinetics were initially made possible using a 19mer peptide photoRNR, which corresponded to the identical 19 residues of the C-terminal tail of $\beta_2$ along with a modification that appended a photooxidant (rhenium phenanthroline [Re]) adjacent to $Y_{356}$ or fluorinated derivatives. This peptide photoRNR enables nucleotide reduction in the presence of $\alpha_2$ and light and allows for observation of radical injection into $\alpha_2$.[21] Radical injection was only realized in the presence of an intact $Y_{731}$–$Y_{730}$ dyad within $\alpha_2$, providing important support for co-linear PCET within this subunit.

More recently, photoRNRs have been generated in which the peptide with the photooxidant is replaced by the full-length $\beta_2$ containing a site-specifically incorporated [Re] photooxidant at residue 355 using a $S_{355}C$-$\beta_2$ mutant.[31] Transient absorption spectroscopy on the active [$Re_{355}$]-$\beta_2$:$\alpha_2$ complex in comparison to the control [$Re_{355}$]-$Y_{356}F$-$\beta_2$:$\alpha_2$ complex allowed for the assignment of a photogenerated $^{\bullet}Y_{356}$.[32] In addition, further modification of [$Re_{355}$]-$\beta_2$ by installation of an unnatural 2,3,5-$F_3$Y in place of $Y_{356}$ in $\beta_2$ yielded the first direct measurement of $^{\bullet}$Y propagation kinetics through the active RNR complex.[33] Comparison of $^{\bullet}$Y decay transient kinetics in the [$Re_{355}$]-2,3,5-$F_3Y_{356}$-$\beta_2$:$\alpha_2$ complex in the presence of substrate, either [3′-$^1$H]-CDP or [3′-$^2$H]-CDP, and effector ATP, revealed an observed rate constant of $1.4 \times 10^4$ $s^{-1}$ and unmasked for the first time an isotope effect on cleavage of the 3′ C–H of the substrate. The photoRNRs thus circumvent the masking of radicals by conformational gating and thus have provided insight regarding radical transport and nucleotide reduction chemistry not accessible by any other method.

In this work, the [Re] photooxidant is attached to Cys in the $Y_{356}C$-$\beta_2$ mutant and this modified [$Re_{356}$]-$\beta_2$ subunit is associated to $\alpha_2$ in which $Y_{731}$ is site-specifically replaced with 2,3,5-$F_3$Y. This [$Re_{356}$]-$\beta_2$:2,3,5-$F_3Y_{731}$-$\alpha_2$ complex together with the [$Re_{356}$]-$\beta_2$:wt-$\alpha_2$ and [$Re_{356}$]-$\beta_2$:$Y_{731}F$-$\alpha_2$ control complexes are studied in the presence of CDP and ATP. In contrast to previous photoRNR systems, installation of [Re] at position 356 enables direct interfacial generation of a tyrosyl radical at position 731. Additionally, by leveraging the greater acidity of 2,3,5-$F_3$Y to enable deprotonation at neutral pH, this residue furnishes an ionizable reporter that varies with experimental pH. In turn, site-selective removal of a single proton at position $Y_{731}(\alpha)$ provides the first protein:protein scaffold of RNR that permits the investigation of the effect of a modified proton microenvironment on radical transport on transient time scales (sub μs) at the interface. In the absence of $Y_{356}$, radical injection is only achieved when position $Y_{731}$ is deprotonated. In addition to confirming the complexity of RNR in maintaining a well-organized PCET pathway, this work introduces and highlights the importance of a well-defined proton exit channel out of $\alpha_2$ involving the key pathway residues, $Y_{356}$ and $Y_{731}$, at the subunit interface.

## Experimental

Modified RNR subunits were constructed, expressed, purified, modified, and characterized as previously reported or with

minor modification.[19,23,24,31,35] Protein concentrations were measured by absorbance at 280 nm using: $\varepsilon_{\alpha_2} = 189\,000\ M^{-1}\ cm^{-1}$, $\varepsilon_{\beta_2\text{-apo}} = 121\,000\ M^{-1}\ cm^{-1}$, $\varepsilon_{\beta_2\text{-holo}} = 131\,000\ M^{-1}\ cm^{-1}$, and $\varepsilon_{\beta_2\text{-[Re]}} = 189\,000\ M^{-1}\ cm^{-1}$. Purity of protein constructs was assessed by SDS-PAGE (Fig. S1†). All measurements were conducted in assay buffer at pH 7.6 (50 mM HEPES, 15 $MgSO_4$, 1 mM EDTA; unless otherwise specified). Measurement of the dissociation constant ($K_D$) between [$Re_{356}$]-$\beta_2$ and wt-$\alpha_2$ was performed by a spectrophotometric competitive inhibition assay as previously reported.[17,21] Measurement of the p$K_a$ of the phenolic proton of 2,3,5-$F_3Y_{731}$ within the assembled 2,3,5-$F_3Y_{731}$-$\alpha_2$:[$Re_{356}$]-$\beta_2$ complex was performed by fluorometric titration as previously reported.[21] The details of methods that deviate from published procedures are provided in the ESI.† Similarly, photoinitiated nucleotide reduction activity assays were performed according to published methods.[17–19,32] Error bars represent $2\sigma$ resulting from photolysis on ≥three independent samples.

Time-resolved spectroscopic measurements were performed using a home-built nanosecond laser system previously described.[21,31–33] Each sample was prepared prior to photolysis and measurements were performed in triplicate. The calculation of the uncertainty in experimental measurements to 95% confidence limits ($2\sigma$) is described in the ESI (eqn S1–S5†).

## Results and discussion

### PhotoRNRs: [$Re_{356}$]-$\beta_2$:$\alpha_2$ and [$Re_{356}$]-$\beta_2$:2,3,5-$F_3Y_{731}$-$\alpha_2$

To probe radical initiation across the $\alpha_2$:$\beta_2$ interface, specific variants of each subunit were required. To directly target the intersubunit radical transport step of $Y_{731}$ oxidation and subsequent radical injection into $\alpha_2$, we chose to circumvent $Y_{356}$ oxidation entirely. In contrast to previous systems where photooxidants were placed adjacent to $Y_{356}$ at position 355, [Re] replaces $Y_{356}$ in this study. The new construct maintains the mutations $C_{268}S$ and $C_{305}S$, and preserves catalytic activity. Additionally, the mutation, $Y_{356}C$, thus enables alkylation with [Re]-Br to yield [$Re_{356}$]-$\beta_2$. To examine the effect of a proton at position $Y_{731}$, this residue was replaced with 2,3,5-$F_3Y$, solution p$K_a$ = 6.4, compared with Y (p$K_a$ = ∼10). The photoRNR construct is illustrated in Fig. 2. These two subunit modifications allow for direct oxidization of $Y_{731}$ by a photo$\beta_2$.

Construction, expression, isolation, and labelling to generate [$Re_{356}$]-$\beta_2$ were performed as previously reported with minor modifications.[31] Unlabelled and reconstituted $Y_{356}C$-$\beta_2$ (holo) is inactive (0.16(5) U) towards nucleotide reduction (wt-$\beta_2$ activity = 6000–8000 U), as expected given the absence of $Y_{356}$. We note that labelling does not preclude binding ($K_D$, = 0.43(11) μM), as measured in the competitive inhibition assay shown in Fig. S2.† This value is in agreement with previously reported values for active photoRNR $\beta_2$ mutants,[32] and not significantly altered from wt-RNR.[12,36]

[$Re_{356}$]-$\beta_2$ displays similar spectroscopic and photophysical properties, as reported previously for [$Re_{355}$]-$\beta_2$.[31] Fig. S3† shows typical absorption and emission spectra for [$Re_{356}$]-$\beta_2$; the absorption spectrum is dominated by the characteristic features of rhenium(I) tricarbonyl bisimine compounds and the emission originates from a triplet metal-to-ligand charge transfer state. The absorption spectrum of [$Re_{356}$]-$\beta_2$ is accurately re-constructed as the sum of $Y_{356}C$-$\beta_2$ and twice the [Re]-Br absorption spectrum, as expected for a construct with two [Re] molecules per $\beta_2$ dimer (Fig. S3†).

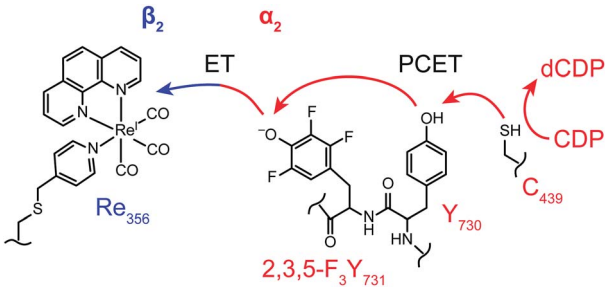


Fig. 2 PhotoRNR design schematic depicting the intersubunit photochemical oxidation of 2,3,5-$F_3Y_{731}$ by [$Re_{356}$]-$\beta_2$, incorporation of 2,3,5-$F_3Y$ at position $Y_{731}$ allowed radical generation to be examined in the absence of a proton at this residue.

Construction of 2,3,5-$F_3Y_{731}$-$\alpha_2$ was achieved using *in vivo* nonsense suppression methodology previously developed to install fluorotyrosine reporters in class Ia RNR.[24] The specific activity of 2,3,5-$F_3Y_{731}$-$\alpha_2$ under catalytic conditions (375(5) U) is diminished relative to wt-$\alpha_2$ (1800–2500 U), while under single-turnover activity (2.75(4) equiv. dCDP/$\alpha_2$) is comparable to wt-$\alpha_2$ (∼3 dCDP equiv./$\alpha_2$). This decrease in catalytic activity, though comparable to that of wild-type (wt), is consistent with previous reports of this mutant.[37]

The deprotonation of 2,3,5-$F_3Y_{731}$ is expected to perturb the rate of radical generation at position $Y_{731}$. The kinetic penalty associated with proton transfer is alleviated by removal of the proton when experimental pH > p$K_a$, thus requiring measurement of the precise p$K_a$ of 2,3,5-$F_3Y_{731}$ in the assembled construct. As previously reported,[19–21,32,33,38] the increase in the rate of photooxidation for tyrosinate relative to tyrosine,[39] makes [Re] emission a reporter of the protonation state of nearby tyrosine residues. Fluorometric titration of the [$Re_{356}$]-$\beta_2$:2,3,5-$F_3Y_{731}$-$\alpha_2$ complex reveals the p$K_a$ of 2,3,5-$F_3Y_{731}$ to be 6.7(1), Fig. 3. Accordingly, ∼90% of 2,3,5-$F_3Y_{731}$ residues are deprotonated under experimental conditions at the optimal operating pH for RNR (pH 7.6). Given the thermodynamically unfavourable acidity of the tyrosyl radical cation (p$K_a$ = −2) a PCET process managing both the electron and proton transfers is mandated.[40,41]

### Photoinitiated substrate turnover

To establish that the photoRNR construct is competent to generate dCDP, the [$Re_{356}$]-$\beta_2$:2,3,5-$F_3Y_{731}$-$\alpha_2$ complex in the presence of [$^3$H]-CDP and ATP was photolyzed for 10 min ($\lambda$ > 313 nm) and dCDP was measured by scintillation counting. The results of this single turnover experiment are shown in Fig. 4. Perturbation of the enzyme by the introduction of [Re] results in a reduced level of turnover that is 5–10% relative to wt-RNR under the same pH conditions. Notwithstanding, the presence of photogenerated products establish the relevance of

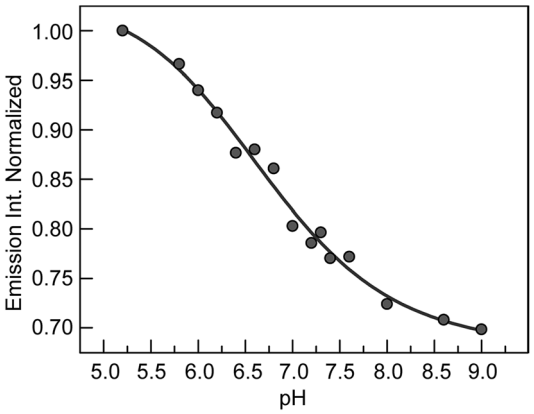


Fig. 3 Measurement of the p$K_a$ of the phenolic proton of 2,3,5-$F_3Y_{731}$ in the [$Re_{356}$]-$\beta_2$:2,3,5-$F_3Y_{731}$-$\alpha_2$ complex by steady-state emission. Fluorometric titrations of 2.5 μM 2,3,5-$F_3Y_{731}$-$\alpha_2$, 3.75 μM [$Re_{356}$]-$\beta_2$, 1 mM CDP, and 3 mM ATP were carried over a pH range of 5 to 9. Samples were illuminated with $\lambda_{exc}$ = 315 nm, scanned from 420–700 nm at 0.5 nm intervals, integrated for 1 s at each data point, and averaged from three scans. The collected emission plots were integrated for fluorescence intensity and plotted against pH. Data were fit to an internal sigmoidal logistic function in OriginPro 8.5. The inflection point of the monoprotic pH-titration curve ($x_0$) is the p$K_a$: $y = A2 + \frac{A1 - A2}{1 + \left(\frac{x}{x_0}\right)^p}$.

[$Re_{356}$]-$\beta_2$:2,3,5-$F_3Y_{731}$-$\alpha_2$ complex to the natural enzyme. Attenuated enzymatic activity is also detected at pH > 7.6 which is consistent with the observed pH rate profiles for the wt enzyme and fluorotyrosine derivatized RNR constructs.[42]

## Radical injection kinetics

The photogeneration of product for the [$Re_{356}$]-$\beta_2$:2,3,5-$F_3Y_{731}$-$\alpha_2$ complex prompted us to undertake radical injection kinetics

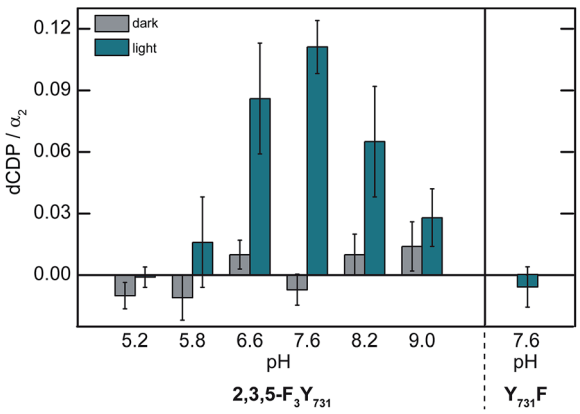


Fig. 4 Photoinitiated nucleotide reduction assay monitored (left) as a function of pH in the [$Re_{356}$]-$\beta_2$:2,3,5-$F_3Y_{731}$-$\alpha_2$ complex and (right) at pH = 7.6 for the control, [$Re_{356}$]-$\beta_2$:$Y_{731}$F-$\alpha_2$. A solution containing 25 μM [$Re_{356}$]-$\beta_2$, 200 μM [$^3$H]-CDP (21 148 cpm nmol$^{-1}$), 3 mM ATP in assay buffer, and a separate solution of 10 μM $\alpha_2$ were incubated at 25 °C. Following two min incubation the two solutions were mixed, transferred to the photolysis cuvette, and illuminated ($\lambda$ > 313 nm) for 10 min.

Table 1 Radical injection rates from [$Re_{356}$]-$\beta_2$ to $\alpha_2$ variants modified at position 731 at pH = 7.6

| [$Re_{356}$]-$\beta_2$: $X_{731}$-$\alpha_2$ | $\tau_{600\ nm\ ns^{-1}}$ [a] | $k_q/10^4\ s^{-1}$ [b] |
|---|---|---|
| **F** | 652(4) | — |
| **Y** | 629(4) | 5.6 (1.4) |
| **2,3,5-$F_3$Y** | 593(6) | 15.4 (2.2) |

[a] Lifetime of emission decay measured on 10 μM [$Re_{356}$]-$\beta_2$, 25 μM $\alpha_2$ (as indicated), 1 mM CDP, 3 mM ATP in assay buffer (pH 7.6), $\lambda_{exc}$ = 355 nm, $\lambda_{obs}$ = 600 nm. Errors shown in parentheses represent 2$\sigma$ resulting from measurement on ≥3 independent samples. [b] Emission quenching rate constant, $k_q$, determined from eqn (1). Error in quenching rate constants calculated as shown in ESI.

studies. Using the [Re]* emission lifetime as a reporter for radical injection, ns TA laser spectroscopy on the [$Re_{356}$]-$\beta_2$:$\alpha_2$ complexes in the presence of CDP and ATP was conducted. The emission decay lifetimes for each construct were measured at pH = 7.6, where maximum turnover was observed, and are summarized in Table 1; representative traces are included in Fig. S4.† As previously observed for [$Re_{355}$]-$\beta_2$,[32] the [Re]* lifetime in [$Re_{356}$]-$\beta_2$ ($\tau$ = 507(3) ns) increases upon binding to $Y_{731}$F-$\alpha_2$ ($\tau_o$ = 652(4) ns), consistent with the more hydrophobic environment engendered by the protein environment. The lifetime $\tau_o$ of the $Y_{731}$F-$\alpha_2$ variant provides a reference for excited-state decay of [Re]* when it is located at the interface, but in the absence of quenching by the tyrosine located at position 731. Upon introduction of $Y_{731}$, the [Re]* emission ($\tau$ = 629(4) ns) is quenched relative to $Y_{731}$F-$\alpha_2$ according to the following equation:

$$k_q = \frac{1}{\tau} - \frac{1}{\tau_0} \quad (1)$$

Accordingly, this quenching rate constant, $k_q$, is equivalent to the radical generation rate, and from eqn (1) it is calculated to

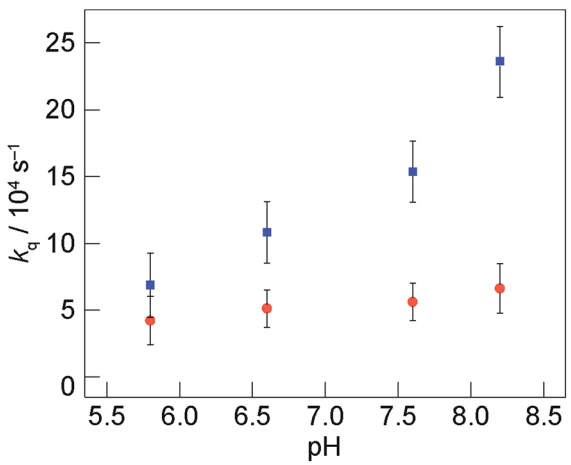


Fig. 5 Quenching rate constant of [Re]* by tyrosine, $k_q$, monitored as function of pH: $Y_{731}$(wt) relative to $Y_{731}$F (●) and 2,3,5-$F_3Y_{731}$ relative to $Y_{731}$F (●). $\tau_o$ corresponds to the lifetime of [$Re_{356}$]-$\beta_2$:$Y_{731}$F-$\alpha_2$. Error bars in $k_q$ represent 2$\sigma$ resulting from error propagation on lifetime measurements as described in ESI.†

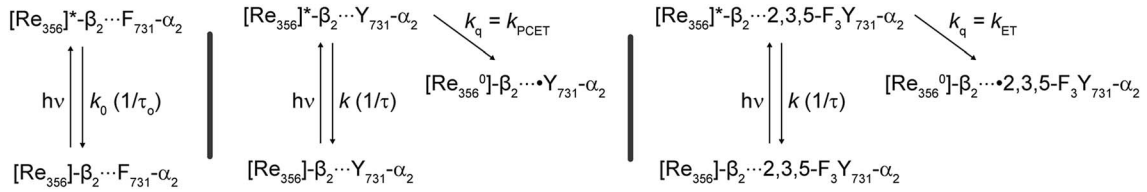


Scheme 1 Excited-state deactivation pathways for $[Re_{356}]$-$\beta_2$ in the presence of indicated $\alpha_2$ subunit.



be 5.6(1.4) × $10^4$ $s^{-1}$. In comparison to previously observed photooxidation of $Y_{356}$ in $[Re_{355}]$-$\beta_2$ ($k_q$ = 4.1(1) × $10^5$ $s^{-1}$), the direct oxidation of $Y_{731}$ by $[Re_{356}]$*-$\beta_2$ is slower possibly owing to an increased charge transfer distance, which is occurring across the subunit interface *vs.* at adjacent positions in previous investigations. Further analysis of the emission decay kinetics of [Re]* reveal a dependency on the rate of radical injection and the protonation state of tyrosine at position $Y_{731}(\alpha)$. Replacement of $Y_{731}$ with 2,3,5-$F_3Y_{731}$ enhances the quenching rate constant by a factor of three ($\tau$ = 593(7) ns ($k_q$ = 15.4(2.2) × $10^4$ $s^{-1}$). This acceleration of radical injection into $\alpha_2$ is in accordance with the differing protonation states of tyrosine in the two constructs. Under the experimental conditions of pH = 7.6, 2,3,5-$F_3Y_{731}$ is deprotonated and hence quenching occurs by ET rather than PCET, which results in faster tyrosine oxidation, despite being ~50–100 mV more difficult to oxidize than native tyrosine at this pH (as determined from solution peak potentials ($E_p$) of N-acetyl and C-amide protected fluorotyrosines measured by differential pulse voltammetry).[22] For clarity, obtaining precise single reside midpoint potentials in protein constructs is extremely challenging, and thus thermodynamic considerations must be guided from these measured $E_p$ values,[11] despite recent findings that suggest significant deviations of the formal reduction potential and solution $E_p$ values.[43]

To investigate how the proton at position $Y_{731}$ affects interfacial PCET and subsequent interfacial radical injection kinetics, emission quenching of the [Re]* within the $[Re_{356}]$-$\beta_2$:2,3,5-$F_3Y_{731}$-$\alpha_2$ complex was monitored over the activity accessible pH region of RNR. A plot of the [Re]* decay lifetimes for $[Re_{356}]$-$\beta_2$ alone and in the three $[Re_{356}]$-$\beta_2$:$\alpha_2$ variant complexes monitored as a function of pH are shown in Fig. S5;† representative emission decay traces are provided in Fig. S4.† The quenching rate constants, $k_q$, as a function of pH may be determined from eqn (1); these rate constants are plotted in Fig. 5. Quenching by $Y_{731}$(wt)-$\alpha_2$ (red circles, ●) and 2,3,5-$F_3Y_{731}$-$\alpha_2$ (light blue squares, ■) are referenced to the control, $Y_{731}F$-$\alpha_2$. Within our error limits, little to no dependence of $k_q$ is observed for the $[Re_{356}]$-$\beta_2$:$Y_{731}$(wt)-$\alpha_2$ complex (●), as native tyrosine is protonated throughout the pH window. Conversely, a large pH dependence is observed for $k_q$ when $[Re_{356}]$-$\beta_2$:2,3,5-$F_3Y_{731}$-$\alpha_2$ is compared to $Y_{731}F$ (■). Guided by our measurement of the p$K_a$ of 2,3,5-$F_3Y_{731}$-$\alpha_2$, shown in Fig. 3, we ascribe the observed differences in quenching to the relative ratio of deprotonated:protonated forms of 2,3,5-$F_3Y_{731}$ as pH is varied. The large $k_q$s at high pH is expected owing to deprotonation of $F_3Y_{731}$ whereas quenching at low pH approaches that of $Y_{731}$ where both of the tyrosines are protonated.

Scheme 1 summarizes the decay pathways for [Re]* in the different variants. The presence of tyrosine introduces an excited-state decay pathway *via* radical generation. For the case of $Y_{731}$(wt)-$\alpha_2$, oxidation occurs by PCET whereas for 2,3,5-$F_3Y_{731}$-$\alpha_2$ occurs by ET. These differing mechanisms of tyrosine oxidation for the two variants in the absence of $Y_{356}$ introduce the possibility that $Y_{356}$ may be involved with facilitating proton removal at the interface, though future experiments are needed to establish its specific role. While a co-linear $Y_{356}$–$Y_{731}$ π-stacked mode where $Y_{356}$ acts directly as the proton acceptor for $Y_{731}$ is unlikely in light of recent Hf EPR/ENDOR data on amino-substituted tyrosine derivatives at various pathway positions, the strongly perturbed $g_x$ values of $NH_2Y_{356}^{\bullet}$ indicate that $Y_{356}$ may communicate with $Y_{731}$ through a network of water molecules.[30] Additional evidence supporting the involvement of $Y_{356}$ in modulating $Y_{731}$ oxidation was also observed in $[Re_{355}]$-$\beta_2$ construct.[32] The photooxidation kinetics of $Y_{731}$, which are summarized in Table S1,† indicate that $Y_{731}$ radical generation is enhanced by the presence of $Y_{356}$ as $[Re_{355}]$-$\beta_2$ oxidation of $Y_{731}$ is 2.1(1.2) times faster for $Y_{356}$ than for $F_{356}$. The presence of $Y_{356}$ may facilitate proton removal from $\alpha_2$ *via* the interface, thus assisting in PCET.

In this directed study, whereby $Y_{356}$ is absent by virtue of its replacement with $[Re_{356}]$, efficient injection of a radical into $\alpha_2$ is realized only when a proton is removed from the pathway by the introduction of 2,3,5-$F_3Y_{731}$. While this result does not implicate $Y_{356}$ directly as the proton acceptor for $Y_{731}$, it supports the contention that $Y_{356}$ is in communication with $Y_{731}$ at the $\alpha_2$:$\beta_2$ subunit interface and that $Y_{356}$ enables the PCET required for efficient radical transport. Further investigations of this contention are underway along with studies to assess the role of possible contributions from other residues, or perhaps metal ions that may also be involved in managing protons at the interface.

## Conclusions

Replacement of $Y_{356}$ by a [Re] photooxidant and installation of 2,3,5-$F_3Y$ at position 731 in $\alpha_2$ furnishes a photoRNR that specifically targets intersubunit radical transport. This construct supports photoinitiated substrate turnover, confirming its fidelity to the natural system. Time-resolved emission studies reveal that 2,3,5-$F_3Y_{731}$ is oxidized at a rate 3 times faster than native $Y_{731}$ even though the non-natural amino acid is thermodynamically more difficult to oxidize at pH 7.6 ($\Delta E_p$ ~ 50–100 mV). These results emphasize the enzymatic imperative for coupling the proton and electron to allow for efficient

radical transport. In conjunction with the parallel studies of $[Re_{355}]$-$\beta_2$, these results suggest the importance of a well-coordinated proton exit channel involving $Y_{356}$ and $Y_{731}$ as key interfacial residues for radical transport across the $\alpha_2$:$\beta_2$ interface.

## Acknowledgements

DYS acknowledges the National Science Foundation's Division of Graduate Education Grant DGE-1144152. PGH thanks the National Institute of Health for a Post-Doctoral Fellowship (GM087034). This research was supported by the U.S. National Institute of Health Grants GM047274 (DGN) and GM029595 (JS).

## Notes and references

1 A. Migliore, N. F. Polizzi, M. J. Therien and D. N. Beratan, *Chem. Rev.*, 2014, **114**, 3381–3645.
2 D. R. Weinberg, C. J. Gagliardi, J. F. Hull, C. F. Murphy, C. A. Kent, B. C. Westlake, A. Paul, D. H. Ess, D. G. McCafferty and T. J. Meyer, *Chem. Rev.*, 2012, **112**, 4016–4093.
3 S. Hammes-Schiffer and A. A. Stuchebrukhov, *Chem. Rev.*, 2010, **110**, 6939–6960.
4 S. Y. Reece and D. G. Nocera, *Annu. Rev. Biochem.*, 2009, **78**, 673–699.
5 J. Barber, *Biochem. Soc. Trans.*, 2006, **34**, 619–631.
6 C. C. Moser, C. C. Page, R. J. Cogdell, J. Barber, C. A. Wraight and P. L. Dutton, *Adv. Protein Chem.*, 2003, **63**, 71–109.
7 J. D. Megiatto Jr, D. D. Mendez-Hernandex, M. E. Tejeda-Ferrari, A. L. Teillout, M. J. Llansola-Portoles, G. Kodis, O. G. Poluektov, T. Rajh, V. Mujica, T. L Groy, D. Gust, T. A. Moore and A. L. Moore, *Nat. Chem.*, 2014, **6**, 423–428.
8 B. A. Barry, *J. Photochem. Photobiol., B*, 2011, **104**, 60–71.
9 J. L. Dempsey, J. R. Winkler and H. B. Gray, *Chem. Rev.*, 2010, **110**, 7024–7039.
10 V. R. I. Kaila, M. I. Verkhovsky and M. Wikstrom, *Chem. Rev.*, 2010, **110**, 7062–7081.
11 E. C. Minnihan, D. G. Nocera and J. Stubbe, *Acc. Chem. Res.*, 2013, **46**, 2524–2535.
12 J. Stubbe, D. G. Nocera, C. S. Yee and M. C. Y. Chang, *Chem. Rev.*, 2003, **103**, 2167–2202.
13 J. Stubbe and W. A. van der Donk, *Chem. Rev.*, 1998, **98**, 705–762.
14 P. E. M. Siegbahn, L. Eriksson, F. Himo and M. Pavlov, *J. Phys. Chem. B*, 1998, **102**, 10622–10629.
15 P. Nordlund and P. Reichard, *Annu. Rev. Biochem.*, 2006, **75**, 681–706.
16 M. Kolberg, K. R. Strand, P. Graff and K. K. Andersson, *Biochim. Biophys. Acta*, 2004, **1699**, 1–34.
17 M. C. Y. Chang, C. S. Yee, J. Stubbe and D. G. Nocera, *Proc. Natl. Acad. Sci. U. S. A.*, 2004, **101**, 6882–6887.
18 S. Y. Reece, M. R. Seyedsayamdost, J. Stubbe and D. G. Nocera, *J. Am. Chem. Soc.*, 2007, **129**, 8500–8509.
19 S. Y. Reece, M. R. Seyedsayamdost, J. Stubbe and D. G. Nocera, *J. Am. Chem. Soc.*, 2007, **129**, 13828–13830.
20 S. Y. Reece, D. A. Lutterman, M. R. Seyedsayamdost, J. Stubbe and D. G. Nocera, *Biochemistry*, 2009, **48**, 5832–5838.
21 P. G. Holder, A. A. Pizano, B. L. Anderson, J. Stubbe and D. G. Nocera, *J. Am. Chem. Soc.*, 2012, **134**, 1172–1180.
22 M. R. Seyedsayamdost, S. Y. Reece, D. G. Nocera and J. Stubbe, *J. Am. Chem. Soc.*, 2006, **128**, 1569–1579.
23 M. R. Seyedsayamdost, C. S. Yee and J. Stubbe, *Nat. Protoc.*, 2007, **2**, 1225–1235.
24 E. C. Minnihan, D. D. Young, P. G. Schultz and J. Stubbe, *J. Am. Chem. Soc.*, 2011, **133**, 15942–15945.
25 M. Eriksson, U. Uhlin, S. Ramaswamy, M. Ekberg, K. Regnström, B. M. Sjöberg and H. Eklund, *Structure*, 1997, **5**, 1077–1092.
26 N. Ando, E. J. Brignole, C. M. Zimanyi, M. A. Funk, K. Yokoyama, F. J. Asturias, J. Stubbe and C. L. Drennan, *Proc. Natl. Acad. Sci. U. S. A.*, 2011, **108**, 21046–21051.
27 E. C. Minnihan, N. Ando, E. J. Brignole, L. Olshansky, J. Chittuluru, F. J. Asurias, C. L. Drennan, D. G. Nocera and J. Stubbe, *Proc. Natl. Acad. Sci. U. S. A.*, 2013, **109**, 39–43.
28 T. U. Nick, W. Lee, S. Koßmann, F. Neese, J. Stubbe and M. Bennati, *J. Am. Chem. Soc.*, 2015, **137**, 289–298.
29 B. Wörsdörfer, D. A. Conner, K. Yokoyama, J. Livada, M. R. Seyedsayamdost, W. Jiang, A. Silakov, J. Stubbe, J. M. Bollinger Jr and C. Krebs, *J. Am. Chem. Soc.*, 2013, **135**, 8585–8593.
30 T. Argirević, C. Riplinger, J. Stubbe, F. Neese and M. Bennati, *J. Am. Chem. Soc.*, 2012, **134**, 17661–17670.
31 A. A. Pizano, D. A. Lutterman, P. G. Holder, T. S. Teets, J. Stubbe and D. G. Nocera, *Proc. Natl. Acad. Sci. U. S. A.*, 2012, **109**, 39–43.
32 A. A. Pizano, L. Olshansky, P. G. Holder, J. Stubbe and D. G. Nocera, *J. Am. Chem. Soc.*, 2013, **135**, 13250–13253.
33 L. Olshansky, A. A. Pizano, Y. Wei, J. Stubbe and D. G. Nocera, *J. Am. Chem. Soc.*, 2014, **136**, 16210–16216.
34 M. R. Seyedsayamdost, C. T. Y. Chan, V. Mugnaini, J. Stubbe and M. Bennati, *J. Am. Chem. Soc.*, 2007, **129**, 15478–15749.
35 J. Ge, G. Yu, M. A. Ator and J. Stubbe, *Biochemistry*, 2003, **42**, 10071–10083.
36 M. C. Y. Chang, Ph.D. Thesis, Dept. of Chemistry, MIT, 2004.
37 E. C. Minnihan, Ph.D. Thesis, Dept. of Chemistry, MIT, 2012.
38 K. Yokoyama, U. Uhlin and J. Stubbe, *J. Am. Chem. Soc.*, 2010, **132**, 8385–8397.
39 T. Irebo, M. T. Zhang, T. F. Markle, A. M. Scott and L. Hammarström, *J. Am. Chem. Soc.*, 2012, **134**, 16247–16254.
40 M. Sjodin, S. Styring, B. Akermark, L. Sun and L. Hammarström, *J. Am. Chem. Soc.*, 2000, **122**, 3932–3936.
41 C. Carra, N. Iordanova and S. Hammes-Schiffer, *J. Am. Chem. Soc.*, 2003, **125**, 10429–10436.
42 M. R. Seyedsayamdost, C. S. Yee, S. Y. Reece, D. G. Nocera and J. Stubbe, *J. Am. Chem. Soc.*, 2009, **131**, 1562–1568.
43 K. R. Ravichandran, L. Liang, J. Stubbe and C. Tommos, *Biochemistry*, 2013, **52**, 8907–8915.

 